


## Original Article

# Predicting abundance indices in areas without coverage with a latent spatio-temporal Gaussian model

Olav Nikolai Breivik <sup>1\*</sup>, Fredrik Aanes<sup>1</sup>, Guldborg Søvik<sup>2</sup>, Asgeir Aglen<sup>2</sup>, Sigbjørn Mehl<sup>2</sup>, and Espen Johnsen<sup>2</sup>

<sup>1</sup>Norwegian Computing Center, Oslo 0373, Norway

<sup>2</sup>Institute of Marine Research, Bergen 5817, Norway

\*Corresponding author: e-mail: [Olavbr@nr.no](mailto:Olavbr@nr.no).

Breivik, O. N., Aanes, F., Søvik, G., Aglen, A., Mehl, S., and Johnsen, E. Predicting abundance indices in areas without coverage with a latent spatio-temporal Gaussian model. – ICES Journal of Marine Science, 78: 2031–2042.

Received 21 December 2020; revised 19 March 2021; accepted 22 March 2021; advance access publication 14 June 2021.

A general spatio-temporal abundance index model is introduced and applied on a case study for North East Arctic cod in the Barents Sea. We demonstrate that the model can predict abundance indices by length and identify a significant population density shift in northeast direction for North East Arctic cod. Varying survey coverage is a general concern when constructing standardized time series of abundance indices, which is challenging in ecosystems impacted by climate change and spatial variable population distributions. The applied model provides an objective framework that accommodates for missing data by predicting abundance indices in areas with poor or no survey coverage using latent spatio-temporal Gaussian random fields. The model is validated, and no violations are observed.

**Keywords:** North East Arctic cod, TMB, Random effects, Matern covariance, Separable covariance

## Introduction

Scientific trawl surveys are conducted worldwide to assess and understand changes in abundance, population structure, and geographical distribution of fish and zooplankton populations (Gunderson, 1993; Wiebe and Benfield, 2003). The surveys are often repeated annually following standard protocols to produce time series, which are used to assess the state of commercially important fish stocks (Gunderson, 1993; Nielsen and Berg, 2014; Miller *et al.*, 2016). In a changing climate, ecosystems and stock distributions are often affected by warming (Richardson, 2008; Fossheim *et al.*, 2015), which is challenging for planning of full survey coverage, and makes it difficult to produce unbiased time series using traditional parametric survey estimation techniques. Lack of survey capacity, changing species distributions, and weather limitations impose a general need of providing abundance predictions in areas with variable and poor survey coverage.

The high North and the Barents Sea is one of the regions which has been dramatically changed by global warming in the last

decades (Fossheim *et al.*, 2015; Lind *et al.*, 2018), and the species distribution and biodiversity are largely impacted (Fossheim *et al.*, 2015; Stenevik and Sundby, 2007). As the largest cod stock in the world the North East Arctic (NEA) cod (*Gadus morhua*) is one of the top predators in this ecosystem, and several studies have shown how the distribution of this cod stock has changed with time in the Barents Sea (Ottersen *et al.*, 1998; Drinkwater, 2005).

A standardized Norwegian-Russian swept area survey has been carried out in the Barents Sea every year since 1981 in January–March (the Barents Sea Winter Survey) (Jakobsen *et al.*, 1997). The survey provides crucial fishery-independent input data for the stock assessment of cod and other fish stocks in the Barents Sea (ICES, 2020). However, the global warming with ensuing spatial shifts in cod distribution and changes in ice coverage has been challenging for a full survey coverage and for survey estimation. In addition, resource limitations and weather conditions have resulted in varying survey coverage between years. Here, we apply a general spatio-temporal model to estimate overall

abundance of cod in the Barents Sea with a focus on predicting abundance with uncertainty in areas with shifting and poor survey coverage. The case study is ideal for testing the applicability of the model due to the shifts in cod distribution and lack of full survey coverage in some years. The model is developed to be applicable for any other swept area surveys.

The applied latent spatio-temporal Gaussian model shares similarities with the commonly used VAST model (Thorson, 2019; Thorson et al., 2020) and the delta-gam model (Berg et al., 2014). The model is particularly similar to VAST, as it uses the same latent spatial Gaussian structure with the stochastic partial differential equation (SPDE) procedure (Lindgren et al., 2011), and includes other dimensions in the latent effect by assuming separability. We therefore highlight that the basic idea behind the model is not new, and our work contributes to broaden the research basis for utilizing spatio-temporal structures in fishery science. Differences between our model and VAST are elaborated in Discussion section. A key difference between our model and the delta-gam model (Berg et al., 2014) is that we include spatio-temporal structures with latent random Gaussian fields.

The main objective of our work is to present and test a statistically sound procedure for survey estimation which accommodates for variable survey coverage over time. The procedure can further be used to identify spatial-temporal dynamics in a changing ecosystem. The article is divided into five sections. Methods section defines the model and abundance prediction procedure. In Inference section, we elaborate the inference procedure. In Case study section, we apply the model in a case study (abundance index of NEA cod based on bottom-trawl data from the joint Russian-Norwegian Barents Sea Winter Survey), investigate an abundance shift, and validate the model. Finally, Discussion section provides discussion and concluding remarks.

**Methods**

The aim of our research is to predict, with uncertainty, abundance indices in any area of a survey domain at any given time. In particular, we want to predict indices in areas with poor or no coverage at any given time within the survey temporal coverage. In this section, we introduce the applied model, and elaborate the prediction procedure.

**Model**

The intuition behind the model is fairly simple, and we will first provide an intuitive interpretation of the model before we introduce it mathematically. All structures are included through a parameter which provides the expected number of fish caught in a haul in year  $y$  at location  $\mathbf{s}$  with length  $l$  (later referred to as  $\mu(y, \mathbf{s}, l)$ ). Note that length can be replaced with age if such data is available. Covariates are included to accommodate for differences in both catchability and abundance. Latent effects in four dimensions are included to accommodate for that observations close to each other in spatio-temporal-length space are typically more similar. The latter part provides the model flexibility to include spatio-temporal-length structures, and by including it as latent Gaussian random fields, we are able to predict abundance by length with uncertainty in areas and years without coverage.

We will now define the model mathematically. Let  $B(y, \mathbf{s}, l)$  be the number of fish in length group  $l$  caught at location  $\mathbf{s}$  in year  $y$ . We assume that  $B(y, \mathbf{s}, l)$  is Poisson distributed, i.e.:

$$P(B(y, \mathbf{s}, l)) = \text{Pois}(B(y, \mathbf{s}, l); \mu(y, \mathbf{s}, l)). \tag{1}$$

Here,  $\text{Pois}(\cdot; \mu)$  represents the Poisson distribution with expectation  $\mu$ . We further assume that

$$\log \mu(y, \mathbf{s}, l) = \beta_{y,l} + \sum_i f_i(x_{y,\mathbf{s},i}) + \alpha(\mathbf{s}, l) + \gamma(y, \mathbf{s}, l) + \psi(y, \mathbf{s}, l) + \log d(y, \mathbf{s}). \tag{2}$$

Here,  $\beta_{y,l}$  is a year and length dependent intercept coefficient,  $x_{y,\mathbf{s},i}$  is the  $i$ th covariate associated with the haul in year  $y$  at location  $\mathbf{s}$ , and  $f_i$  is a function of the corresponding covariate. Furthermore,  $\alpha$  and  $\gamma$  are latent spatial-length and spatio-temporal-length mean zero Gaussian random effects. Finally,  $\psi$  is a latent mean zero Gaussian random haul effect (a nugget effect) with correlation structure across length within hauls, and  $d(y, \mathbf{s})$  is an offset providing the distance trawled.

The latent effect  $\alpha$  in (2) is intended to accommodate for a stationary spatial-length field, and  $\gamma$  accommodates for time varying fluctuations around the stationary spatial-length field. We assume that both these effects are latent Gaussian with separable covariance structures. The corresponding correlation structures are further assumed to be stationary Matern in space (Stein, 2012) and with separate first order auto regressive (AR1) structures in both time and length. The latent haul effect  $\psi$  is intended to accommodate for an unexplained variation within each haul (intra haul correlation), and is included with an AR1 correlation structure in length dimension. The correlation structures of the latent effects are thereby expressed as:

$$\begin{aligned} \text{Cov}(\alpha(\mathbf{s}_1, l_1), \alpha(\mathbf{s}_2, l_2)) &= \rho_{\alpha,l}^{||l_1-l_2||} \frac{\sigma_{\alpha}^2}{2^{\nu-1}\Gamma(\nu)} \\ &\quad \times (\kappa_{\alpha} ||\mathbf{s}_1 - \mathbf{s}_2||)^{\nu} K_{\nu}(\kappa_{\alpha} ||\mathbf{s}_1 - \mathbf{s}_2||) \\ \text{Cov}(\gamma(y_1, \mathbf{s}_1, l_1), \gamma(y_2, \mathbf{s}_2, l_2)) &= \rho_{\gamma}^{||y_1-y_2||} \rho_{\gamma,l}^{||l_1-l_2||} \frac{\sigma_{\gamma}^2}{2^{\nu-1}\Gamma(\nu)} \\ &\quad \times (\kappa_{\gamma} ||\mathbf{s}_1 - \mathbf{s}_2||)^{\nu} K_{\nu}(\kappa_{\gamma} ||\mathbf{s}_1 - \mathbf{s}_2||) \\ \text{Cov}(\psi(y_1, \mathbf{s}_1, l_1), \psi(y_2, \mathbf{s}_2, l_2)) &= \begin{cases} \sigma_{\psi}^2 \rho_{\psi,l}^{||l_1-l_2||}, & \text{if } \mathbf{s}_1 = \mathbf{s}_2 \text{ and } y_1 = y_2, \\ 0, & \text{else.} \end{cases} \end{aligned} \tag{3}$$

Here,  $\rho_{\gamma}$ ,  $\rho_{\alpha,l}$ ,  $\rho_{\gamma,l}$ , and  $\rho_{\psi,l}$  are autocorrelation parameters,  $\sigma_{\alpha}^2$ ,  $\sigma_{\gamma}^2$ , and  $\sigma_{\psi}^2$  are marginal variances,  $\kappa_{\alpha}$  and  $\kappa_{\gamma}$  are spatial scale parameters,  $||\cdot||$  is the Euclidean distance measure in km,  $\nu$  is a smoothing parameter and  $K_{\nu}(\cdot)$  is the modified Bessel function of the second kind. We fix  $\nu = 1$  since this value is typically poorly identifiable (Blangiardo and Cameletti, 2015, page 194).

The covariates are included with two different types of splines. For a covariate that we believe the corresponding effect has a cosine shape, we include it with a Fourier approximation (Lay, 2006) with one basis function. The Fourier approximation is defined as:

$$f(x) = \beta_1 \sin(x) + \beta_2 \cos(x), \tag{4}$$

where  $x \in [0, 2\pi)$  represents the covariate and  $\beta_1$  and  $\beta_2$  are parameters estimated. The other covariates are included with p-splines. The applied p-spline procedure includes the regression

coefficients as latent variables and includes one penalization parameter  $\lambda$  (Wood, 2017, p. 239).

### Predicting indices

The predicted indices are obtained by integrating  $\mu(y, \mathbf{s}, l)$  over the area of interest. Meaning that the predicted index in area  $A$  is

$$I_{A,y,l} = \frac{|A|}{n_i} \sum_{\mathbf{s}^* \in \{A\}} \mu(y, \mathbf{s}^*, l), \quad (5)$$

where  $\{A\}$  is the set of all  $n_i$  integration points in  $A$  and  $|A|$  is the area of  $A$ . Supplementary Figure S1 illustrates the evenly distributed integration points applied in our case study. When predicting indices, the offset in (2) is set to one, meaning that  $\mu$  in (5) is the predicted catch per unit effort.

### Centre of gravity

A spatial shift in abundance is investigated with the *centre of gravity* (COG) measure, which is a widely used measure for spatial distribution shifts (Thorson and Barnett, 2017; Thorson et al., 2016; Pinsky and Palumbi, 2014). Several studies indicate that Arctic fish species have lately shifted north in the Barents Sea (Frainer et al., 2017; Eriksen et al., 2017; Fosheim et al., 2015; Jakobsen and Ozhigin, 2011). The COG for a given length and year is defined as:

$$\text{COG}_{y,l} = \left( \frac{\sum_{\mathbf{s}^* \in \{S\}} \mu(y, \mathbf{s}^*, l) \text{lon}_{\mathbf{s}^*}}{\sum_{\mathbf{s}^* \in \{S\}} \mu(y, \mathbf{s}^*, l)}, \frac{\sum_{\mathbf{s}^* \in \{S\}} \mu(y, \mathbf{s}^*, l) \text{lat}_{\mathbf{s}^*}}{\sum_{\mathbf{s}^* \in \{S\}} \mu(y, \mathbf{s}^*, l)} \right), \quad (6)$$

where  $\{S\}$  is the set of all integration points and  $(\text{lon}_{\mathbf{s}^*}, \text{lat}_{\mathbf{s}^*})$  is the Universal Transverse Mercator (UTM) coordinates of integration point  $\mathbf{s}^*$ .

### Inference

The model is implemented with use of the R-package *TMB* (Kristensen et al., 2016) and the optimization routine *nlmminb* in the R-package *stats* (R Core Team, 2019). *TMB* is a freely available R-package and is well suited for performing fast inference with latent Gaussian models. *TMB* automatically differentiates the likelihood and utilizes Markov structures to efficiently integrate over the latent variables with the Laplace approximation.

To perform fast inference with high dimensional Gaussian random fields, it is essential to represent their precision matrices as a sparse matrices efficiently. Note that the covariance structures in time and length dimension are AR1, and the corresponding sparse precision matrix can be found in e.g. Cressie and Wikle (2011, p. 170). The spatial correlation structure is obtained with the SPDE-procedure introduced in Lindgren et al. (2011). This procedure introduces nodes in a relatively fine discretization in space and represents an approximate Matern covariance structure between the nodes with a sparse precision matrix. How many spatial nodes that are needed depends on the spatial range in the specific case study (the distance in which the correlation is approximately 0.1). Figure 1 shows the spatial resolution of the mesh used in our case study, and the nodes are the corners of the triangles (144 nodes). The latent effect at any location inside the triangles are defined as a convex combination of the effects at its corners (standard linear interpolation) (Lindgren et al., 2011).

### Spatial mesh

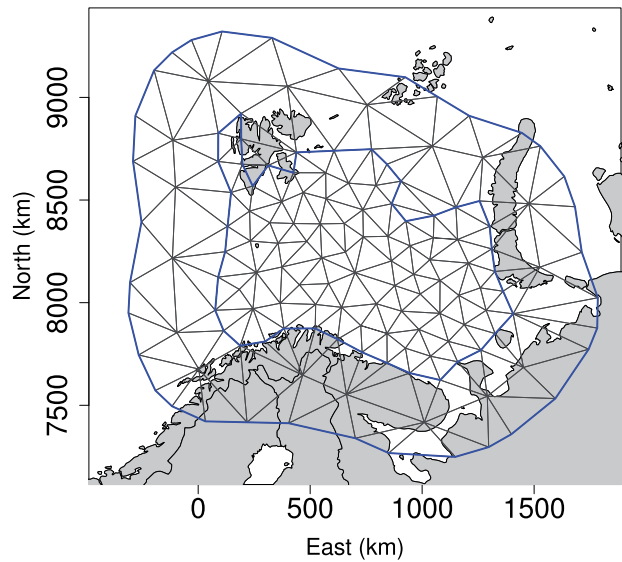


**Figure 1.** Mesh used when approximating the spatial correlation structure. The map is shown with projection UTM 35.

Key structures from R-INLA (Rue et al., 2009) are used when calculating the sparse spatial precision matrix in *TMB*. Effects on results by applying a finer spatial resolution are discussed in Discussion section, and the effects are observed to be minor in our case study.

Even though we utilize sparse structures, the spatio-temporal-length ( $\gamma$ ) and the spatial-length ( $\alpha$ ) effects are computationally demanding to estimate. To reduce computation complexity, we therefore represent these latent effects with a lower length resolution compared to in observation space. The representation is constructed by defining both  $\gamma$  and  $\alpha$  with the structure (3) at a set of knots in length dimension. We further define a latent effect between two knots by standard linear interpolation. Note that a similar procedure is conducted in space where the spatial discretization is illustrated in Figure 1. By representing  $\gamma$  and  $\alpha$  with such an approximation, computation complexity is reduced because the number of latent effects that are integrated over with the Laplace approximation within the inference procedure is reduced. In our case study, we include every third length group as a knot (starting at the shortest group). Effects on results by not conducting this approximation is discussed in Discussion section, and the effects are observed to be minor in our case study.

Indices (5) and COG (6) are defined as non-linear functions of the random effects. Estimates of these quantities may be substantially biased if predicted random effects are inserted directly (Thorson and Kristensen, 2016). The bias correcting routine (Thorson and Kristensen, 2016) implemented in *TMB* is therefore applied when providing point estimates of indices and COG. In a geostatistical case study for predicting abundance indices investigated in Thorson and Kristensen (2016), it was observed an approximately constant correction factor across years. In our case study, however, we observe a time varying correction factor. Uncertainty intervals are calculated by standard Gaussian approximations of log-indices, COG, and internally represented model parameters. Internal representation of model parameters are provided in Table A1 in the Appendix. The bias correction routine

for the variance estimates (Thorson and Kristensen, 2016) is not conducted because of computational reasons.

### Case study

As a case study, we predict abundance indices by length for NEA cod based on data from the joint Russian-Norwegian Winter Survey. The main objective in this research is to predict indices in areas without coverage, and there are several years with poor coverage in this survey time series.

### Data

Survey data for the period 1994–2019 are analysed in this study. Older data are not included as the trawl selectivity changed in 1994 when the mesh-size in the cod-end was reduced from approximately 40 mm to 22 mm (Mehl *et al.*, 2016). Data preparation was carried out using the survey estimation software StoX (Johnsen *et al.*, 2019) with the same data and setting as used for the official survey time series (Mehl *et al.*, 2016). The survey area is divided into 26 strata, and bottom trawl haul positions are depicted for 2007 and 2014 (Figure 2), which are examples of years with poor and good coverage, respectively. The trawl positions in each stratum are decided using a fixed grid where the distance between stations is dependent on the historical fish density distributions, see Mehl *et al.* (2016) for details. All hauls have been carried out with a standard research bottom trawl, and standard tow duration was 30 min in 1994–2010, and 15 min thereafter (Mehl *et al.*, 2016). Generally, the entire catch is sorted in catch samples by species. For big catches, a sub-sample of the catch is taken. The total length of cod is measured by cm for all individuals in the catch sample. For large catch samples consisting solely of small cod (<20 cm), 50 individuals are length measured. In our analyses, the response is number of cod by 5 cm length groups. In accordance to the official survey estimation procedure, the catches are adjusted for length dependent catchability (Mehl *et al.*, 2016). The adjustment scales the catch at length with a constant (at cm level) and treats these numbers as

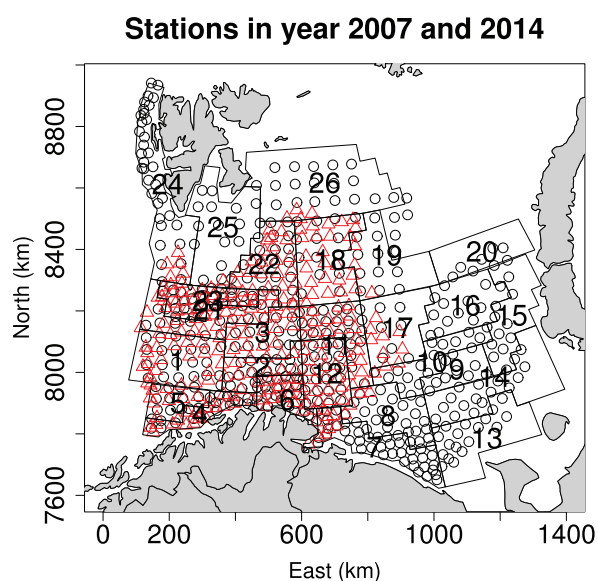


**Figure 2.** Illustration of station locations in year 2007 (red triangles) and 2014 (black circles). The polygons define the survey domain with numbered strata.

observed catches when producing indices used in the current assessment of NEA cod (ICES, 2020). Our model needs the response as integers, and the scaled catches are therefore rounded off to the nearest integer. The length groups are defined from 20 to 100 cm, where the last group consists of all cod longer than or equal to 100 cm. When referring to a length group, we refer to the shortest length in the length group for brevity. Table 1 provides a short description of the data. Trawl haul locations in all years are provided in Supplementary Figure S2.

### Covariates

Two covariates are included in our case study. It has been observed that NEA cod behaviour changes during the day (Hjellvik *et al.*, 2002), and we therefore included sun altitude as a covariate. It is reasonable that the effect of sun altitude has a cosine type of shape, and we therefore included the effect with a Fourier approximation (4). The sun altitude covariate is defined between 0 and  $2\pi$ , where both 0 and  $2\pi$  represents the lowest possible sun altitude at the given location and date, while  $\pi$  represents the corresponding highest altitude. Every value between 0 and  $\pi$  is a linear transformation of the sun altitude in the period the sun is rising, and every value between  $\pi$  and  $2\pi$  is a linear transformation of the altitude while the sun is setting. Note that sun altitude is a covariate for catchability, index predictions provided are standardized to the time of day when the sun is at its highest.

It has previously been observed that depth has a predictive effect for abundance of NEA cod (Fall *et al.*, 2018). We therefore included depth as a covariate with use of p-splines. The depth is defined as the average of minimum and maximum depth observed during the haul. We have truncated depth to be between 100 and 400 m to avoid including rare depths. The depth at each integration point is assumed equal to the observed depth at the closest station. Five basis functions are used in the p-spline (Wood, 2017, p. 239).

### Model selection

For model selection, the procedure recommended in Zuur (2009) is used. First the correlation structures are selected using all relevant covariates, followed by a selection of significant covariates using the selected correlation structure. Table 2 shows AIC-values with different combinations of latent effects. The option to include all random effects is favoured by AIC and is therefore used further in our case study. Note that the option to include the spatio-temporal-length effect *without* the length correlated haul effect is not in Table 2. With that option the spatial range in the spatio-temporal-length effect is estimated much shorter, which results in that the spatial mesh should be defined in such a high resolution that the model is not estimable within reasonable computational time.

Two covariates, depth and sun altitude, are investigated. Table 3 shows obtained AIC values with different combinations of the covariates when using the selected covariance structure. We see that both covariates are clearly favoured by AIC.

### Results

Estimated sun altitude effect is illustrated in Figure 3a. All illustrated effects are for expected catch on log scale (2), meaning that the difference of 0.4 observed in Figure 3a is equivalent with an approximate  $(e^{0.4} - 1) * 100\% \approx 50\%$  increase in catch rate from night to day. A similar observation of higher catch rates during

daytime has also been observed for NEA cod bycatch in the Barents Sea shrimp fishery (Breivik *et al.*, 2016a). This effect may be caused by the tendency of zooplankton to aggregate closer to the bottom (where the trawl is conducted) during daytime

**Table 1.** Short summary of data used.

Data	Description
Year	Survey data are included for the years 1994–2019.
Stations (hauls)	On average 338 stations every year, varies between 177 and 534.
Location	The coordinates of each station.
Number of cod	The number of cod observed in each length group at each station
Depth	The depth at each station. On average 263 m, with 94 to 438 m as 90% coverage interval.
Time in day	Local start time for each haul, can be at any time in day.

**Table 2.** Obtained AIC with different combinations of latent effects.

Random effects included	Parameters	AIC
No random effects	445	1966961
Spatial-length ( $\alpha$ )	448	1422135
Haul ( $\psi$ )	447	464110
Spatial-length and haul ( $\alpha$ and $\psi$ )	450	447222
Spatio-temporal-length and haul ( $\gamma$ and $\psi$ )	451	438153
All random effects	454	<b>438068</b>

Lowest AIC is written in bold.

**Table 3.** Obtained AIC with different combinations of covariates.

Covariates	Parameters	AIC
No covariates	451	439127
Sun altitude	453	438868
Depth	452	438355
Sun altitude and depth	454	<b>438068</b>

Lowest AIC is written in bold.

(Jakobsen and Ozhigin, 2011) which may result in better food conditions for NEA cod. Estimated depth effect is illustrated in Figure 3b. The density of NEA cod is estimated to be highest at depths of around 200 m and decreases in both directions. The linear predictor increases with approximately 1 when moving from 100 m to 200 m depth, meaning that expected catch rate increases approximately  $(e^1 - 1) * 100\% \approx 170\%$ .

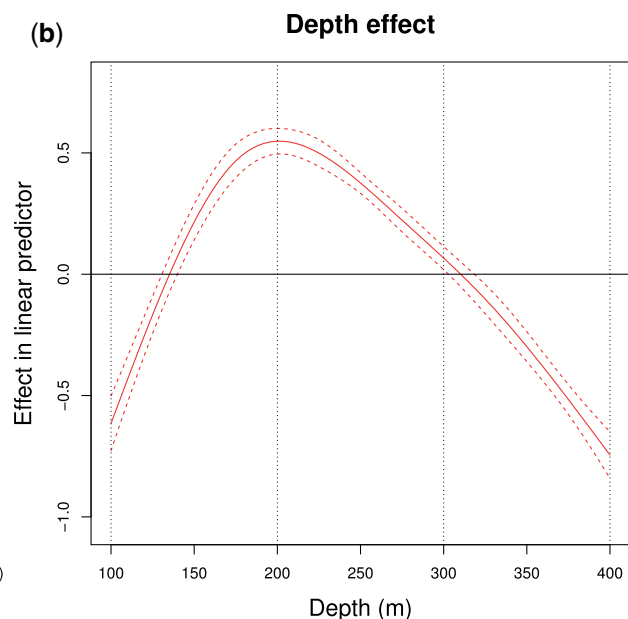
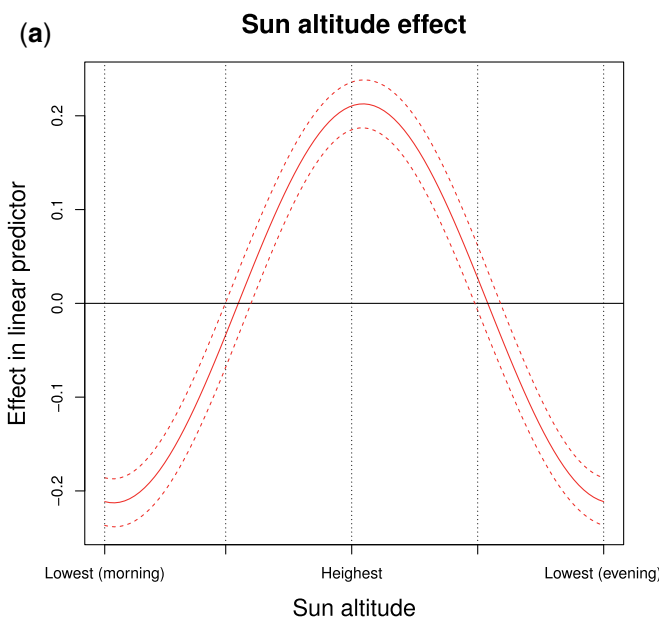
Table 4 shows estimated model parameters. Note that we find clear evidence for correlation structures in all dimensions of the latent effects. The spatial scale parameter in the spatial-length effect imposes a range of  $\frac{\sqrt{8}}{0.0034} \approx 830$  km, and in the spatio-temporal-length effect it imposes a range of  $\frac{\sqrt{8}}{0.0088} \approx 320$  km.

Figure 4 shows estimated spatio-temporal effect ( $\gamma$ ) for length group 60 cm added to the corresponding yearly varying intercept coefficients. We observe that the model estimates clear similarities between years, which can be used when predicting abundance indices in areas without coverage. Relative spatial differences in catch rates between years can be calculated with the formula  $(e^{\Delta} - 1) * 100\%$ , where  $\Delta$  is the linear predictor difference.

The main objective of our research is to predict abundance indices in areas without survey coverage. The eastern part of the Barents Sea (strata 7, 8, 9, 10, 13, 14, 15, 16, 17, and 20) has in several years not been fully covered, and Figure 5 shows the estimated index per year for four length groups in this area. The survey coverage was particularly poor in the years 1997, 1998, 1999,

**Table 4.** Estimated model parameters. Numbers in parentheses are 95% confidence intervals.

Parameter	Estimate	Parameter	Estimate
$\sigma_{\alpha}$	2.60 (2.01, 3.36)	$\sigma_{\gamma}$	1.55 (1.43, 1.68)
$\sigma_{\psi}$	1.12 (1.11, 1.14)	$\kappa_{\alpha}$	0.0034 (0.0026, 0.0044)
$\kappa_{\gamma}$	0.0088 (0.0079, 0.0097)	$\rho_{\alpha,l}$	0.96 (0.93, 0.97)
$\rho_{\gamma,l}$	0.89 (0.87, 0.90)	$\rho_{\psi,l}$	0.89 (0.886, 0.893)
$\rho_t$	0.80 (0.77, 0.83)	$\lambda$	0.0099 (0.0027, 0.035)



**Figure 3.** Estimated sun altitude effect (a) and depth effect (b). Intervals represent 95% confidence intervals.

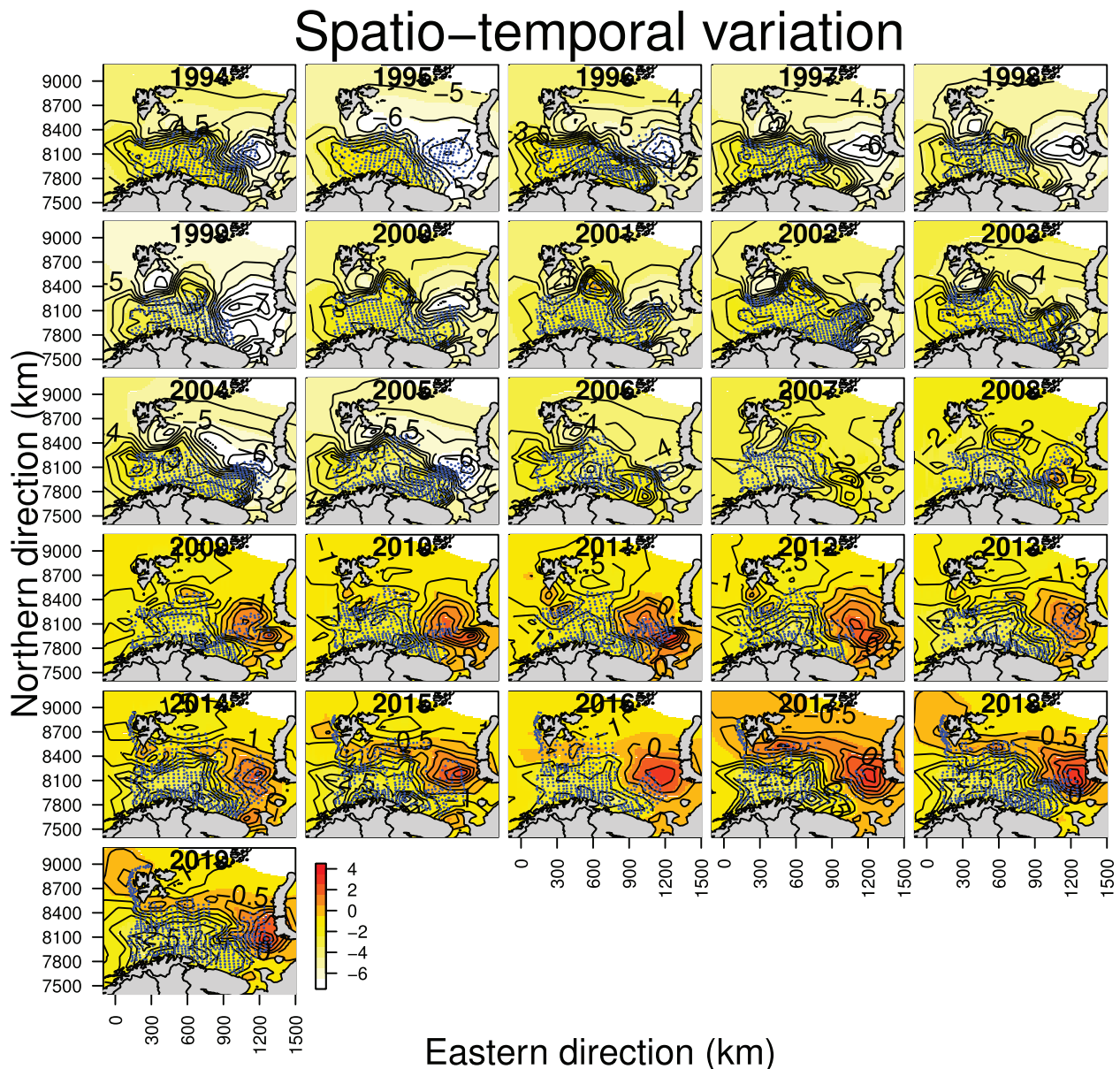


**Figure 4.** Estimated latent spatio-temporal effect added the yearly varying intercept coefficient for length group 60 cm in year 1994–2019. Blue points illustrate station locations within each year.

and 2007. We manage to predict the indices in years with poor coverage, but typically with relatively larger uncertainty.

Figure 6 illustrates predicted abundance per length, where the size of the bubbles are proportional to the index on natural scale. Cohort-structures are visible, especially from a cohort entering the system around year 2005. Since the index is per length, we cannot say exactly which cohort this structure comes from, but it is likely the 2004 and 2005 cohorts which are observed to be exceptionally strong (ICES, 2019, Table 3.16). Furthermore, a time varying bias correction factor (Thorson and Kristensen, 2016) for the indices (5) is observed, see Supplementary Figure S3 for an illustration.

### Spatial shift in abundance

Spatial shift in the NEA cod abundance is investigated with the COG measure (6). Figure 7 shows 95% confidence areas for COG in every second year for several length groups. We observe that there is a clear significant spatial shift in northern direction for the small cod, and in northeast direction for larger cod. No covariates are included which can explain such a spatial shift, and the result is purely data driven through the latent structure. Note that we do not accommodate for geometric anisotropy, see e.g. Thorson and Haltuch (2019), but the shape of the confidence contours in Figure 7 varies because the estimated spatio-temporal-length effect varies between years.

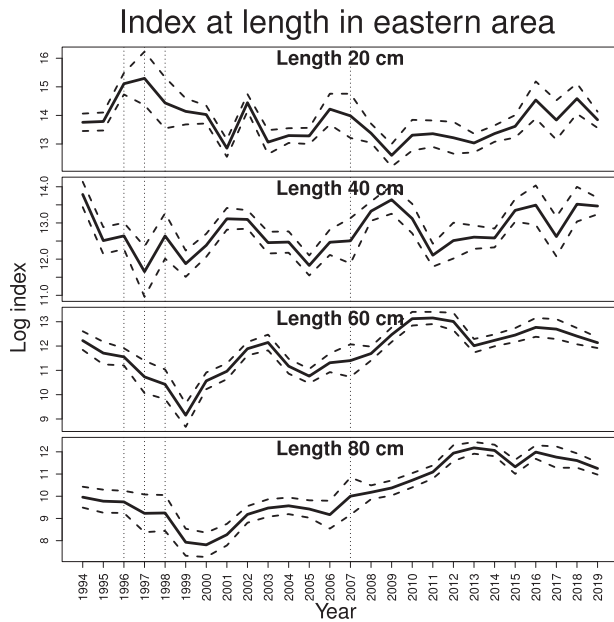


**Figure 5.** Predicted log indices with 95% prediction intervals in the eastern part of the Barents Sea for length group 20, 40, 60, and 80 cm. Vertical dashed lines illustrate years with particularly poor coverage in the eastern part of the survey area.

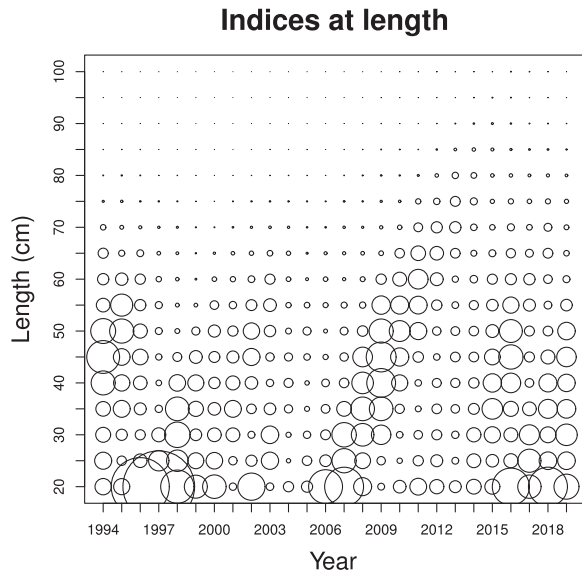


**Figure 6.** Predicted indices at length, size of bubbles are proportional to the predicted index.

**Validation**

One-step ahead (OSA) residuals (Thygesen *et al.*, 2017) are investigated to identify model assumption violations. Figure 8a illustrates standard normal quantile plot of OSA residuals and we observe no model assumption violations (e.g. prediction bias or wrong prediction uncertainty). Figure 8b illustrates empirical autocorrelation of the OSA-residuals, and we observe no unexplained correlation structures. Figure 8c and d shows similar plots when the random effects (3) are neglected, and we observe clear model assumption violations. The violations observed when

neglecting the random effects confirm the importance of including the latent structure. For computational reasons, the OSA residuals are only calculated for the most recent 50 hauls, which consists of 850 observations in year 2019. The OSA calculation procedure provides an ordering of the observations, and sequentially predicts one observation given all previous observations (Thygesen *et al.*, 2017). We have chosen to first predict the observation corresponding to the shortest length in a haul, then proceed to observations from the same haul in increasing length order. The next observation is further chosen from a haul that is typically close in both space and time.

A simulation experiment is performed to confirm that the model is able to estimate itself. The simulation experiment is performed by fixing the model parameters to their maximum likelihood estimates, and simulate realizations of the latent spatio-length, spatio-temporal-length, and nugget effect. We further simulate realizations of observations through (1). Supplementary Figure S4 shows parameter estimates obtained with ten simulated data sets. We observe that the model is able to estimate itself.

Sensitivity to starting values is investigated by fitting the model with different initial values, and comparing the obtained indices, parameters, and likelihood with the corresponding values obtained in Results section. The different starting values are selected as those applied in Results section with an independent mean zero Gaussian random variable with standard deviation 0.2 added to each internal parameter (including latent effects). We fitted the model ten times with different starting values, and the maximum difference between both log indices and log likelihood was approximately  $10^{-5}$ . This indicates that the results are stable with respect to starting values. The indices compared are not bias corrected for computational reasons. The largest difference observed for the effects in the linear predictor (2) and parameters in the correlation structures (3) was approximately  $10^{-3}$ , which indicates that the global maximum likelihood estimates are found.

A leave-out study is performed to validate if spatio-temporal-length structures improve prediction. The study is conducted by sequentially leaving out all observations in the eastern area (strata 7, 8, 9, 10, 13, 14, 15, 16, 17, and 20) in each year. Catch per length group in test sets are predicted with the bias correction procedure (Thorson and Kristensen, 2016). Two of the model formulations are compared: including only the haul nugget effect vs. including all random effects. Figure 9 shows predicted log mean catch per length group in each year obtained with the simplified and full model. We observe that the model including all random effects clearly has more predictive power. Corresponding mean sum of square residuals are 0.82 and 0.45 with the simplified and full model, respectively.

**Computational features**

Computational complexity is a challenge when performing inference with high dimensional latent Gaussian fields. Even though we utilize sparse structures in the precision matrices, the inference is time consuming. The inclusion of the spatio-temporal-length random field implies that we need to solve a  $144 * 26 * 7 = 26208$  dimensional integral several times with the Laplace approximation, which is the models computational bottle neck. Estimating the selected model takes approximately 4 h in our case study (with use of an Intel Zenon E4-2630 2.4Ghz, and utilizing one core). We want to highlight that the computation time is

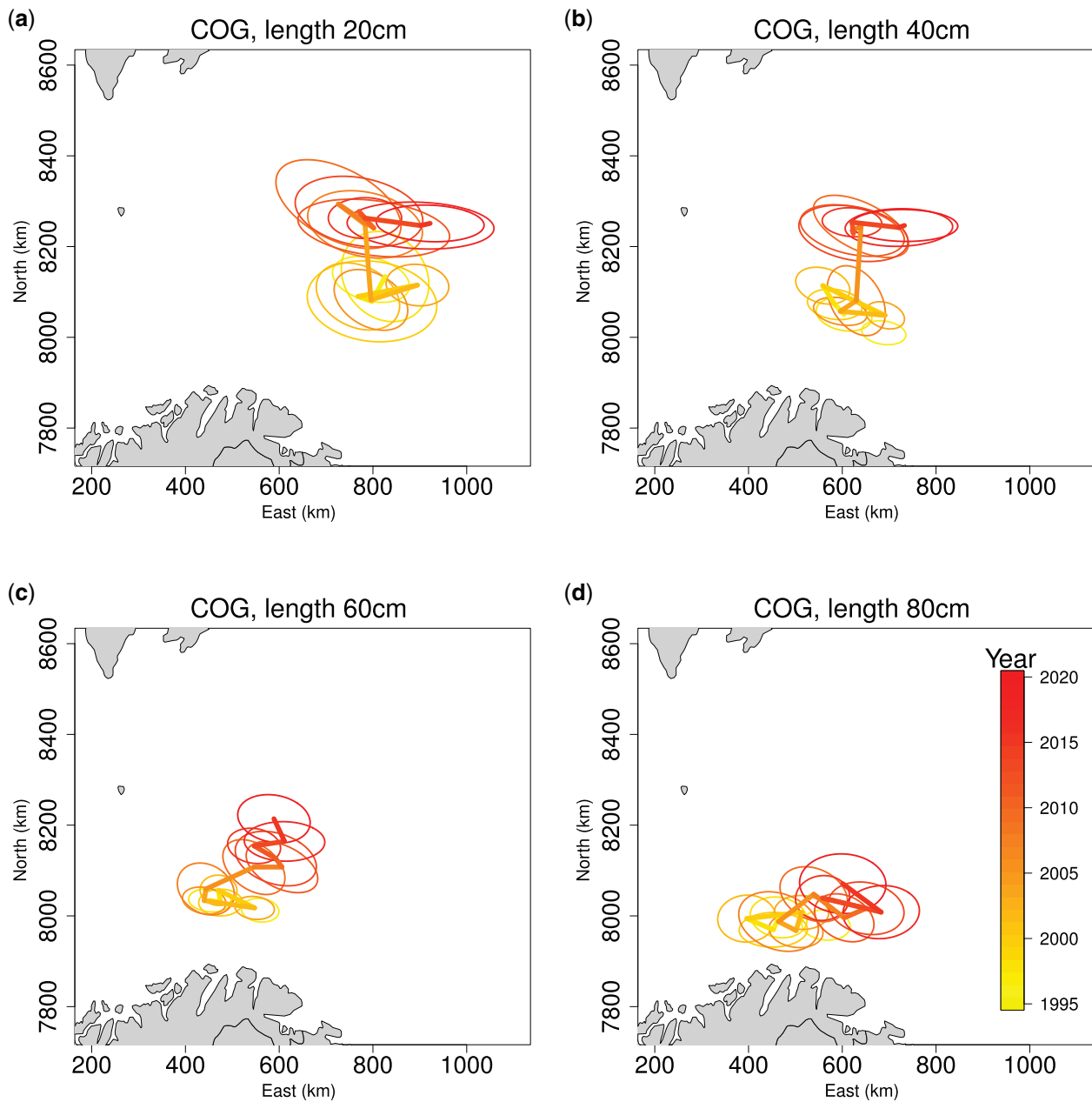


**Figure 7.** Estimated 95% confidence areas for COG in every second year for length group 20 cm (a), 40 cm (b), 60 cm (c), and 80 cm (d). Coloured lines illustrate corresponding point estimates.

dependent on the linear algebra library R uses. Microsoft R Open 3.5.1 (<https://mran.microsoft.com/open>) was used when performing inference within 4 h. We further want to highlight that all regression coefficients are estimated in the inner optimization with the profile functionality in TMB, this procedure was conducted because it provided faster inference. Providing bias corrected indices based on the estimated model took approximately 3 h.

## Discussion

In this research, we applied a general latent spatio-temporal-length Gaussian model for predicting abundance indices. In particular, we predicted indices in areas without survey coverage. We

illustrated that the model finds significant structures in the data, which can be used to provide abundance predictions in areas without coverage. The model output is not limited to abundance indices used for assessment purposes, it can equally well be used to estimate the centre of gravity by length. In accordance with previous studies (Fossheim *et al.*, 2015; Eriksen *et al.*, 2017), we found a significant northeasterly shift in the distribution of NEA cod, and the magnitude and direction of the spatial shift differ between length groups. The model was validated, and no clear warning was observed.

The northern and eastern shift in the cod distribution illustrated in Figure 7 is purely data driven through the latent spatio-temporal-length effect. A reasonable explanation for the observed shift is



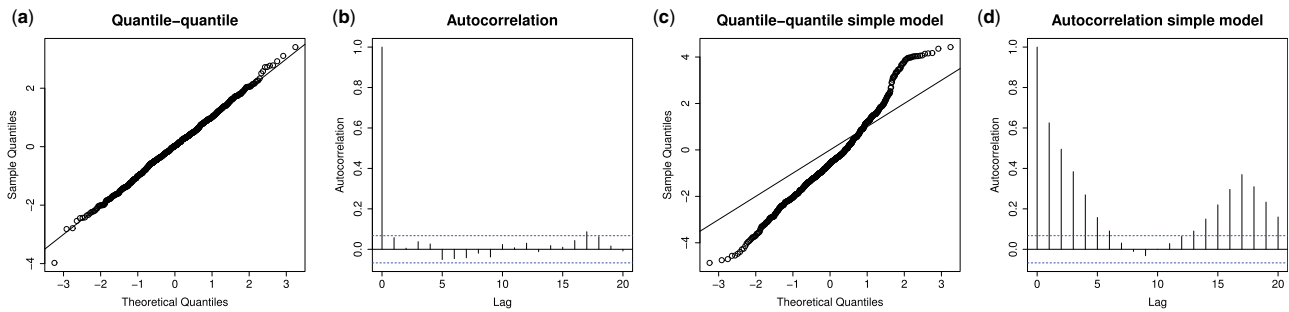


**Figure 8.** Normal quantile–quantile plot of one-step ahead (OSA) residuals with final model (a) and without latent effects (c). Empirical correlation between OSA residuals with final model (b) and without latent effects (d). Blue dashed lines are 95% confidence intervals when assuming independence.

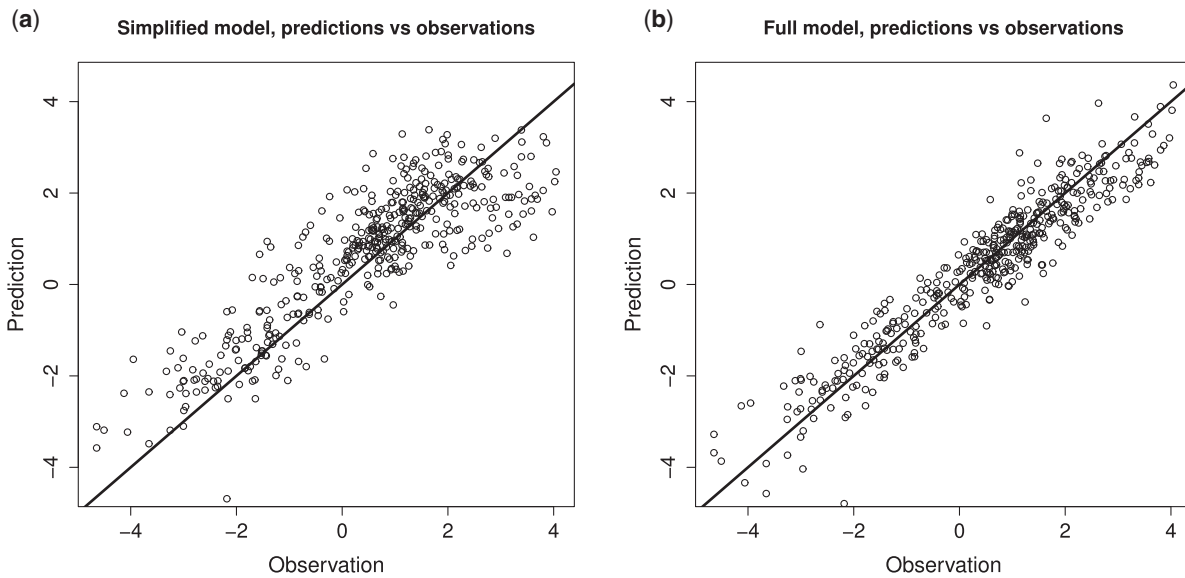


**Figure 9.** Predictions vs. observations of log mean catch per length group within each test sets with simplified model (a) and full model (b). Lines illustrate where predictions are equal observations.

climate change and warming of the Barents Sea. In winter (when the survey is conducted), the distribution of cod is mainly concentrated at temperatures above 1°C (Jakobsen and Ozhigin, 2011, p. 227), and it is argued that cod biomass will increase because of climate change due to higher plankton production in a sea with less ice (Jakobsen and Ozhigin, 2011, p. 796). A reasonable causal hypothesis is therefore that the spatial change in plankton production due to changing ice conditions has provided better living conditions for cod in the northeastern part of the Barents Sea.

The nugget effect,  $\psi$ , is included with correlation across lengths within hauls to accommodate for intra haul correlation structures. If  $\psi$  is replaced with a length independent nugget effect, the spatial range in the spatio-temporal-length effect is estimated much shorter in our case study. It is intuitive that the spatial range in the spatio-temporal-length effect decreases if we remove the correlation in the nugget effect. The model then sacrifices structures between hauls to include structures within hauls through the spatio-temporal-length effect.

The correlation structure in space is approximated with the SPDE procedure (Lindgren *et al.*, 2011), with use of a mesh

consisting of 144 nodes (see Figure 1). Ideally, the results should be unaffected by applying a finer spatial resolution. This is however not computational feasible, the applied mesh is based on a weighted selection of computation speed and how detailed the Matern covariance structure is represented. We investigated the effect of increasing the spatial resolution to 275 nodes (see Supplementary Figure S5). The computation time then increased from 4 h to approximately 17 h. Corresponding obtained model parameters are provided in Supplementary Table S1. We observe that the estimates are only slightly affected. The corresponding mean difference between log bias-corrected indices across all length groups and years is 0.0075, and the mean absolute difference is 0.025. The small differences for both parameter estimates and abundance indices provide a strong case for that the applied spatial resolution is satisfactory in our case study.

The correlation structure in length dimension is included with an AR1 structure. To reduce computation complexity, we represented the spatio-temporal-length and spatial-length effects with lower resolution in length dimension compared to in observation space. We have investigated the effect of not applying such an approximation, and thereby marginalizing overall length groups in

the inference procedure with the Laplace approximation. The computation time then increased from 4 h to approximately 45 h. The corresponding mean difference between log bias-corrected indices across all length groups and years is  $-0.0030$ , and the mean absolute difference is  $0.020$ . Corresponding obtained model parameters are provided in [Supplementary Table S2](#). We observe that the model parameters are slightly affected. The small differences between parameter estimates and indices indicate that the approximation has minor effects on our results. In our case study, the estimated autocorrelation parameters in length dimension are  $0.89$  and  $0.96$  for  $\gamma$  and  $\alpha$ , respectively. Since the model detects such strong correlations in length dimension, we find it intuitively reasonable that the results are minor affected by representing the latent spatio-temporal-length and spatial-length effects with a lower length resolution.

All covariates included in the model are length independent, meaning that the effect is equal for all length groups. For each covariate, we investigated including one effect for the shortest fish, and one for the longest fish, and apply linear interpolation to define effects of length in between. [Supplementary Figure S6](#) illustrates the effect for the shortest and longest cod. Both covariates are observed to have an approximately similar effect across length. We therefore do not include length dependent covariates in (2), and highlight that it is possible within the modelling framework.

We investigated including an additional zero-probability as  $\pi_0(\mathbf{s}, y, l) = \text{Pois}(0; \beta_0^{(\pi)} + \beta_1^{(\pi)} \mu(\mathbf{s}, y, l))$ , where  $\beta_0^{(\pi)}$  and  $\beta_1^{(\pi)}$  are parameters estimated and  $\mu$  is the expectation parameter in (1). However, including such a structure introduced convergence issues in our case study. By manually investigating the data, we observed that zeroes almost always occur when neighbouring observations are either zero or small. This observation indicates that zero-observations typically occur when the expectation in (1) is small, which provides a strong case for that an additional zero probability is not of major importance in our case study. We do not investigate the inclusion of such a structure further. However, we want to highlight that it is possible to include an additional zero-probability in the modelling framework, either through a linear combination of the expectation parameter in (1) or through a separate independent linear predictor ([Thorson \*et al.\*, 2020](#)).

Abundance indices used in the current ICES-assessment of NEA cod ([ICES, 2020](#)) accommodate for poor survey coverage (in a given year) by scaling the observed index in a subjectively selected area that includes observations. The scaling factor is defined as the ratio between the index in the uncovered area and in the selected area in neighbouring years ([Mehl \*et al.\*, 2016](#)). The procedure is based on subjective decisions regarding which areas to apply the procedure and what we define as neighbouring years. By using the suggested model, we avoid including any year specific subjective assumptions.

The differences between our applied model and VAST are in the details, both models apply separable latent Gaussian random fields, and include these random effects through linear predictors in standard observation distributions. Here, we list all features in our model that to our knowledge have not been applied with use of VAST. (i) A length dimension in the spatial and spatio-temporal correlation structure, see (3). For example, [Thorson and Haltuch \(2019\)](#) include data on length, but without correlation structures across lengths within these latent effects. Note that the inclusion of length in the spatio-temporal effect increases the

computational complexity exponentially, we therefore included the length dimension in these latent effects with a lower resolution compared to in observation space. (ii) A nugget effect is included with correlation structure across length within each haul (intra haul correlation). It was important to include such a nugget effect in our case study to satisfactorily accommodate for spatio-temporal-length structures. (iii) Covariates are included with use of Fourier approximations and p-splines. (iv) Separate spatial scale parameters are included for the random effects, see  $\kappa_x$  and  $\kappa_y$  in (3). Since these four differences are in the finer details, we want to highlight that our work also validates the framework that VAST is based on to predict abundance indices.

The correlation structures for the latent effects are assumed to be AR1 in both time and length dimension. Note that this implies a stationary assumption, and it may be the case that some pairs of length groups are differently correlated even though they are equally separated. [Berg and Nielsen \(2016\)](#) accommodate for possible different correlation between neighbouring ages by defining the distances in between the ages as model parameters. We leave for future research to investigate if non-stationary correlation structures can improve the model.

Our work apply the introduced model for assessment purposes, and we want to highlight that the model can be used in other fields within fisheries science. By applying the model, we have an approximation available for how a species of interest is distributed in relatively fine spatio-temporal-length resolution, and how catchability is affected by covariates. [Breivik \*et al.\* \(2016b\)](#) applied a recruitment index as a covariate when predicting bycatch of juvenile NEA cod in the Barents Sea shrimp fishery. Our introduced model can be applied to e.g. provide a spatio-temporal varying index covariate for bycatch prediction. Furthermore, [Jakobsen and Ozhigin \(2011, p. 227\)](#) stated that NEA cod avoids temperatures below  $1-2^\circ\text{C}$  during winter. Such a hypothesis can be validated by including bottom sea temperature in (2) if such data are available.

Currently, fish stock assessment is divided into two main parts. The first part consists of producing time series of abundance indices, and the second part consists of including these time series in an assessment model. Our research contributes to the first of these two parts. For future research, it would be interesting to replace observations in assessment models with predictions from a spatio-temporal index model and estimate both models simultaneously. As we see it, a computational challenge with such an approach is that the conditional independence structure between latent effects (3) within a year and neighbouring years is no longer present because of the population dynamic structure.

## Supplementary data

[Supplementary material](#) is available at the *ICESJMS* online version of the manuscript.

## Data availability

Code used to produce all results are available at <https://github.com/OlavNikolaiBreivik/ICESpaperSpatioTemporal2020>. Only data collected by Norwegian vessels are provided at GitHub. Access to the Russian data set may be granted upon inquiry to the Federal State Budget Scientific Institution ‘‘Russian Federal Research Institute of Fisheries and Oceanography.’’

## Acknowledgements

We want to thank the Polar branch of Russian Federal Research Institute of Fisheries and Oceanography (“PINRO” named after N.M. Knipovich) and the Norwegian Institute of Marine Research, and their staff, for collecting the data used in our research. We also want to thank Anders Nielsen at DTU-aqua for general TMB specific discussions, which was helpful for overcoming several obstacles we encountered. The research was funded by the Norwegian Institute of Marine Research through the project 3680\_14809 (REDUS). We also want to thank two anonymous reviewers for constructive comments.

## Funding

The research was funded by the Norwegian Institute of Marine Research through the project 3680\_14809 (REDUS).

## Authors' contributions

Olav Nikolai Breivik: Developing the modelling idea, implementing it and writing the article. Fredrik Aanes: Valuable parts of the implementation, discussion and review. Guldborg Søvik: Discussion and review. Asgeir Aglen: Discussion and review. Sigbjørn Mehl: Discussion and review. Espen Johnsen: Discussion, help with data, review and writing parts of the introduction.

## References

- Berg, C. W., and Nielsen, A. 2016. Accounting for correlated observations in an age-based state-space stock assessment model. *ICES Journal of Marine Science*, 73: 1788–1797.
- Berg, C. W., Nielsen, A., and Kristensen, K. 2014. Evaluation of alternative age-based methods for estimating relative abundance from survey data in relation to assessment models. *Fisheries Research*, 151: 91–99.
- Blangiardo, M., and Cameletti, M. 2015. *Spatial and Spatio-temporal Bayesian Models with R-INLA*. Chichester: John Wiley & Sons.
- Breivik, O. N., Storvik, G., and Nedreaas, K. 2016a. Latent Gaussian models to decide on spatial closures for bycatch management in the Barents Sea shrimp fishery. *Canadian Journal of Fisheries and Aquatic Sciences*, 73: 1271–1280.
- Breivik, O. N., Storvik, G., and Nedreaas, K. 2016b. Latent Gaussian models to estimate historical bycatch in commercial fishery.
- Cressie, N., and Wikle, C. K. 2011. *Statistics for Spatio-temporal Data*. New Jersey: John Wiley & Sons.
- Drinkwater, K. F. 2005. The response of Atlantic cod (*Gadus morhua*) to future climate change. *ICES Journal of Marine Science*, 62: 1327–1337.
- Eriksen, E., Skjoldal, H. R., Gjørseter, H., and Primicerio, R. 2017. Spatial and temporal changes in the Barents Sea pelagic compartment during the recent warming. *Progress in Oceanography*, 151: 206–226.
- Fall, J., Ciannelli, L., Skaret, G., and Johannesen, E. 2018. Seasonal dynamics of spatial distributions and overlap between Northeast Arctic cod (*Gadus morhua*) and capelin (*Mallotus villosus*) in the Barents Sea. *PLoS One*, 13: e0205921.
- Fossheim, M., Primicerio, R., Johannesen, E., Ingvaldsen, R. B., Aschan, M. M., and Dolgov, A. V. 2015. Recent warming leads to a rapid borealization of fish communities in the arctic. *Nature Climate Change*, 5: 673–677.
- Frainer, A., Primicerio, R., Kortsch, S., Aune, M., Dolgov, A. V., Fossheim, M., and Aschan, M. M. 2017. Climate-driven changes in functional biogeography of Arctic marine fish communities. *Proceedings of the National Academy of Sciences*, 114: 12202–12207.
- Gunderson, D. R. 1993. *Surveys of Fisheries Resources*. New York: John Wiley & Sons.
- Hjellvik, V., Godø, O. R., and Tjøstheim, D. 2002. Diurnal variation in bottom trawl survey catches: does it pay to adjust? *Canadian Journal of Fisheries and Aquatic Sciences*, 59: 33–48.
- ICES 2019. Report of the Arctic Fisheries Working Group, 24–30 April, Lisbon.
- ICES 2020. Arctic Fisheries Working Group (AFWG), ICES Scientific Reports. 2: 577. pp. ICES CM/ACFM.
- Jakobsen, T., Korsbrekke, K., Mehl, S., and Nakken, O. 1997. Norwegian combined acoustic and bottom trawl surveys for demersal fish in the Barents Sea during winter. ICES Document CM 1997/Y: 17. 26 pp.
- Jakobsen, T., and Ozhigin, V. K. 2011. *The Barents Sea-Ecosystem, Resources, Management. Half a Century of Russian-Norwegian Cooperation*. Tapir Akademisk Forlag.
- Johnsen, E., Totland, A., Skålevik, Å, Holmin, A.J., Dingsør, G. E., Fuglebakk, E., and Handegard, N. O. 2019. StoX: An open source software for marine survey analyses. *Methods in Ecology and Evolution*, 10: 1523–1528.
- Kristensen, K., Nielsen, A., Berg, C. W., Skaug, H., and Bell, B. M. 2016. TMB: automatic differentiation and Laplace approximation. *Journal of Statistical Software*, 70: 1–21.
- Lay, D. C. 2006. *Linear Algebra and Its Applications*, 3rd edn. Boston: Person.
- Lind, S., Ingvaldsen, R. B., and Furevik, T. 2018. Arctic warming hotspot in the northern Barents sea linked to declining sea-ice import. *Nature Climate Change*, 8: 634–639.
- Lindgren, F., Rue, H., and Lindström, J. 2011. An explicit link between Gaussian fields and Gaussian Markov random fields: the stochastic partial differential equation approach. *Journal of the Royal Statistical Society: Series B (Statistical Methodology)*, 73: 423–498.
- Mehl, S., Aglen, A., and Johnsen, E. 2016. Re-estimation of swept area indices with CVs for main demersal fish species in the Barents Sea winter survey 1994–2016 applying the Sea2Data StoX software. *Fisken og Havet*, 10: 44.
- Miller, T. J., Hare, J. A., and Alade, L. A. 2016. A state-space approach to incorporating environmental effects on recruitment in an age-structured assessment model with an application to southern New England yellowtail flounder. *Canadian Journal of Fisheries and Aquatic Sciences*, 73: 1261–1270.
- Nielsen, A., and Berg, C. W. 2014. Estimation of time-varying selectivity in stock assessments using state-space models. *Fisheries Research*, 158: 96–101.
- Ottersen, G., Michalsen, K., and Nakken, O. 1998. Ambient temperature and distribution of north-east arctic cod. *ICES Journal of Marine Science*, 55: 67–85.
- Pinsky, M. L., and Palumbi, S. R. 2014. Meta-analysis reveals lower genetic diversity in overfished populations. *Molecular Ecology*, 23: 29–39.
- R Core Team 2019. *R: A Language and Environment for Statistical Computing*. R Foundation for Statistical Computing, Vienna, Austria.
- Richardson, A. J. 2008. In hot water: zooplankton and climate change. *ICES Journal of Marine Science*, 65: 279–295.
- Rue, H., Martino, S., and Chopin, N. 2009. Approximate Bayesian inference for latent Gaussian models by using integrated nested Laplace approximations. *Journal of the Royal Statistical Society: Series B (Statistical Methodology)*, 71: 319–392.
- Stein, M. L. 2012. *Interpolation of Spatial Data: Some Theory for Kriging*. New York: Springer Science & Business Media.
- Stenevik, E. K., and Sundby, S. 2007. Impacts of climate change on commercial fish stocks in norwegian waters. *Marine Policy*, 31: 19–31.
- Thorson, J. T. 2019. Guidance for decisions using the Vector Autoregressive Spatio-Temporal (VAST) package in stock, ecosystem, habitat and climate assessments. *Fisheries Research*, 210: 143–161.
- Thorson, J. T., Adams, C. F., Brooks, E. N., Eisner, L. B., Kimmel, D. G., Legault, C. M., Rogers, L. A., et al. 2020. Seasonal and interannual variation in spatio-temporal models for index standardization and phenology studies. *ICES Journal of Marine Science*, 77: 1879–1892.

Thorson, J. T., and Barnett, L. A. 2017. Comparing estimates of abundance trends and distribution shifts using single- and multispecies models of fishes and biogenic habitat. *ICES Journal of Marine Science*, 74: 1311–1321.

Thorson, J. T., and Haltuch, M. A. 2019. Spatiotemporal analysis of compositional data: increased precision and improved workflow using model-based inputs to stock assessment. *Canadian Journal of Fisheries and Aquatic Sciences*, 76: 401–414.

Thorson, J. T., and Kristensen, K. 2016. Implementing a generic method for bias correction in statistical models using random effects, with spatial and population dynamics examples. *Fisheries Research*, 175: 66–74.

Thorson, J. T., Pinsky, M. L., and Ward, E. J. 2016. Model-based inference for estimating shifts in species distribution, area occupied and centre of gravity. *Methods in Ecology and Evolution*, 7: 990–1002.

Thygesen, U. H., Albertsen, C. M., Berg, C. W., Kristensen, K., and Nielsen, A. 2017. Validation of ecological state space models using the Laplace approximation. *Environmental and Ecological Statistics*, 24: 317–339.

Wiebe, P. H., and Benfield, M. C. 2003. From the hensen net toward four-dimensional biological oceanography. *Progress in Oceanography*, 56: 7–136.

Wood, S. N. 2017. *Generalized Additive Models: An Introduction with R*. Boca Raton: CRC Press.

Zuur, A. F. 2009. *Mixed Effects Models and Extensions in Ecology with R*. New York: Springer.

*Handling editor: Stan Kotwicki*

**Appendix**

Uncertainty intervals of model parameters are constructed by a standard Gaussian approximations of its internal representations. The transformations are provided in [Table A1](#).

**Table A1.** Transformation used in the optimization routine,  $x$  refers to the corresponding internal representation.

Parameter	Transformation
$\sigma_\alpha, \sigma_\gamma, \sigma_\psi, \kappa_\alpha, \kappa_\gamma$ and $\lambda$	$\log x$
$\rho_{\alpha,l}, \rho_{\gamma,l}, \rho_{\psi,l}$ and $\rho_t$	$\frac{2}{1+\exp(-2x)} - 1$